Check for updates

View Article Online
View Journal

CrystEngComm

Accepted Manuscript

This article can be cited before page numbers have been issued, to do this please use: A. Valimukhametova, A. Khannanov, A. Kiiamov, I. Vakhitov, I. Gilmutdinov, F. Vagizov and A. Dimiev, *CrystEngComm*, 2019, DOI: 10.1039/C9CE00580C.

This is an Accepted Manuscript, which has been through the Royal Society of Chemistry peer review process and has been accepted for publication.

Accepted Manuscripts are published online shortly after acceptance, before technical editing, formatting and proof reading. Using this free service, authors can make their results available to the community, in citable form, before we publish the edited article. We will replace this Accepted Manuscript with the edited and formatted Advance Article as soon as it is available.

You can find more information about Accepted Manuscripts in the author guidelines.

Please note that technical editing may introduce minor changes to the text and/or graphics, which may alter content. The journal's standard Terms & Conditions and the ethical guidelines, outlined in our author and reviewer resource centre, still apply. In no event shall the Royal Society of Chemistry be held responsible for any errors or omissions in this Accepted Manuscript or any consequences arising from the use of any information it contains.

ROYAL SOCIETY OF CHEMISTRY

rsc.li/crystengcomm

View Article Online
DOI: 10.1039/C9CE00580C

ARTICLE

Growth of the invar nanoparticles on the graphene oxide support

Alina Valimukhametova,[a,b] Artur Khannanov,[a] Airat Kiiamov,[a] Iskander Vakhitov,[a] Ildar Gilmutdinov,[b] Farit G. Vagizov,[b*] and Ayrat M. Dimiev[a*]

Received 00th January 20xx,
Accepted 00th January 20xx

DOI: 10.1039/x0xx00000x

Binary nanoparticles, composed from two different metals, attract significant attention because they possess properties not typical for respective single-component nanoparticles. In bulk form, iron and nickel form an alloy called invar in which the two metals are mixed in the ratio Fe:Ni = 2:1. In this work, we demonstarte formation of the alloyed nanoparticles of invar, as opposed to the theoretically possible formation of the particles of the two individual metals. The formation of the alloyed nanoparticles is conducted in the two-step process: liquid phase impregntaion of graphene oxide with the salts of the metals, and sussequent annealing of the as-formed dry composite. Unlike the solution phase reaction conditions, in this approach, the binary nanoparticles are assembled in conditions, where the metals atoms are immobilized on the surface of the decomposing graphene oxide, and at temperatures significantly lower than the melting points of the two metals. The structure of the as-grown nanocrystals is investigated by Mössbauer spectroscopy, powder X-ray diffrcation, X-ray photoelectron spectroscopy, and scanning electron microscopy. Majority of the Fe/Ni nanoparticles are in a magnetically ordered state, and the composite is a soft magnet.

1. Introduction

Metal nanoparticles (NP) on a structural support have become a class of interesting materials from perspectives of energy storage systems,[1] catalysis,[2] and biomedical applications.[3, 4] In recent years, significant attention was given to the nanoparticles composed from two different metals. Such nanoparticles open the doors to a large variety of materials with exact chemical composition and desired properties, not available in single-component materials or structures.

Normally, binary nanoparticles of two metals are produced by gas phase and liquid phase reactions.[5] Progress in the gas phase synthesis was made mostly by sputtering alloyed materials.[6] Thus, Xu et al.[7] reported formation of iron– silver (Fe–Ag) and cobalt–gold (Co–Au) NPs with the core–shell structures, obtained by the sputtering of FeAg and CoAu composite targets, respectively.

The liquid phase method involves preparation of nanoparticles from metal salts in aqueous and non-aqueous solutions. The factors affecting formation of bimetallic NPs are the bond strength, nanoparticle's surface energy, electronegativity and atomic radii. For substitutional solid solutions the difference in atomic radii between the two elements should be less than 15%.[8, 9] Fe/Ni alloys are well suited for these characteristics, and, therefore, have attracted significant attention.[10] The bulk Fe/Ni alloys can be obtained in the broad Fe/Ni ratio that influences their properties. Thus, these alloys have intriguing anomalies of some physical characteristics in the region of the iron content between 60% and 70% (the invar region). The invar alloy has a very low coefficient of thermal expansion. Therefore, it is used in applications where high dimensional stability is required (e.g. precision measuring instruments, aerospace control devices, telescopes, ring laser gyroscopes, etc.).[11-15] Fe/Ni alloys are one of the most widely used soft magnetic materials because of their high saturation magnetization (Ms) and high Curie temperature.[16, 17] For industrial purposes, the bulk invar alloy is produced by melting two metals in the ratio of Fe:Ni = 2:1.

From the fundamental science perspectives, it is interesting to investigate if the mixed alloyed nanocrystals will be formed on the nano-level, at conditions very different from the industrial processing of the bulk substances, and at the temperatures significantly lower than the melting points of the two metals. In particular, it is interesting to investigate if the alloyed NPs will be formed on the surface of a structural support such as graphene oxide (GO). In the article[18] authors showed formation of the Fe/Ni nanoparticles (Fe/Ni-NP) on reduced GO (RGO) by the wet chemical route. In that work, the metal salts were mixed with the GO suspension, and the reductant N_2H_4 was introduced. Subsequently, Fe^{3+} and Ni^{2+} ions were reduced and deposited from solution in situ, forming tiny Fe/Ni nanocrystallites on the surface of reduced graphene oxide. When metal NPs are obtained by thermal annealing, the reaction conditions and the mechanism of the NP growth are very different from that of the liquid phase processing.[19, 20] In

[a] Laboratory for Advanced Carbon Nanomaterials, Kazan Federal University. E-mail: AMDimiev@kpfu.ru, Ayrat M. Dimiev;
[b] Institute of Physics, Kazan Federal University, Kremlyovskaya str. 18, Kazan 420008, Russian Federation. E-mail: vagizovf@gmail.com; Farit G. Vagizov

Electronic Supplementary Information (ESI) available: [details of any supplementary information available should be included here]. See DOI: 10.1039/x0xx00000x

Published on 11 June 2019. Downloaded by Kazan State University on 6/18/2019 8:28:08 AM.

CrystEngComm Accepted Manuscript

View Article Online
DOI: 10.1039/C9CE00580D

this case, metal ions evenly cover the surface of GO as a nearly monoatomic layer, being chemically bound to the GO's functional groups. Subsequently, they are reduced being immobilised on the surface, simultaneously with decomposition of GO, which turns to the thermally processed GO (tpGO). Unlike solution phase reaction,[18] NPs cannot grow by deposition of new ions/atoms from solution, where they have high mobility. To form NPs, metal atoms must migrate along the surface of the structural support.[19] The main task of this study was to investigate if the thermal annealing of the mixed Fe/Ni-GO composite will lead to formation of the alloyed Fe/Ni nanocrystals, or NPs of the individual metals will be formed.

Herein, we demonstrate the possibility of obtaining the alloyed binary metal nanoparticles on the surface of graphene oxide by the annealing-reduction approach.

2. Experimental

2.1 Synthesis of graphene oxide

Graphite flakes (5.15 g) were dispersed in 96% sulfuric acid (600 mL) at room temperature, and stirred for 1 hour. Then, 1 wt. equiv. of $KMnO_4$ (5.15 g) was added. The mixture became green due to the formation of the oxidizing agent MnO^{3+}. Additional portions of $KMnO_4$ (5.15 g each) were added when the green colour of MnO^{3+} was vanished, indicating that the oxidizing agent was consumed. A total of 4 wt. equiv. of $KMnO_4$ were sequentially added. The end of the oxidation was determined by the disappearance of the green colour after each $KMnO_4$ addition. After complete consumption of $KMnO_4$, the reaction was quenched with 1000 mL of ice-water mixture, and then H_2O_2 solution (9 mL, 30%) was added to convert manganese by-products to soluble colourless Mn (II) ions. The reaction mixture was centrifuged 1 hour at 5000 rpm to separate GO from acid. For purification, the GO precipitate was redispersed in distilled water, stirred 1 hour, and centrifuged 1 hour at 5000 rpm to separate purified GO from washing waters. This constituted one purification cycle. Four more purification cycles were performed consecutively: one time with distilled water and three times with HCl (4%). The GO precipitate after the last washing was dried in air. 8.5 g of air-dried GO was obtained.

2.2 Preparation of Fe^{3+}/Ni^{2+}-GO composite (impregnation step)

In a typical procedure, a $Fe(NO_3)_3$ solution (100 mL, 0.1%) and $Ni(NO_3)_2$ solution (100 mL, 0.7%) were added to GO solution (800.0 mL, 0.1%) with stirring. The dispersion was further stirred on a magnetic stirrer for 1 hour. The resulted dispersion was centrifuged ~2 hours at 5000 rpm until complete separation of the reaction product, and the supernatant was decanted. For purification, the jelly Fe^{3+}/Ni^{2+}-GO precipitate was redispersed in 800 mL DI water, stirred for 4 hours and centrifuged as above. The purified jelly samples were dried at ambient condition and used as the air-dried solid samples.

2.3 The growth of Fe/Ni-NPs (annealing)

The air-dried Fe^{3+}/Ni^{2+}-GO sample, was introduced into the tube furnace, purged with nitrogen to remove all the oxygen, and was heated to 210°C with 3°C/min heating rate. The sample was maintained at 210°C for 15 min. Then the sample was heated to 900°C with 3°C/min rate and maintained at this temperature for 20 min. The obtained product is denoted as Fe/Ni-NP_tpGO.

2.4 Characterization of obtained samples

The powder X-ray diffraction (XRD) was acquired with Bruker D8 Advance with Cu Kα irradiation (λ=1.5418 Å) in the Bragg-Brentano geometry; the rate was 0.18˚/min; the range of 2θ angle was from 7˚ through 100˚; the step was 0.015˚. The thermogravimetric analysis (TGA) data was collected with the STA 449 F5 Jupiter analyzer from Netzsch in both Ar and synthetic air atmosphere. The scanning electron microscopy (SEM) images were acquired with a field-emission high resolution scanning electron microscope Merlin from Carl Zeiss at accelerating voltage of incident electrons of 5 kV and a current probe of 300 pA. The X-ray photoelectron spectroscopy (XPS) spectra were acquired in a UHV chamber of the multi-technique surface analysis system Phoibos 100/150 from SPECS. The Mg Kα X-ray source operated at 12.5 kV and 250 W was used. A pass energy of 30 eV (step size of 0.5 eV) was used for wide range scans; pass energy of 20 eV (step size of 0.1 eV) was used for high resolution measurements. All spectra were analyzed by using the CasaXPS software. The Mössbauer effect measurements were carried out mainly at room temperature, using a conventional constant-acceleration spectrometer, produced by WissEl (Germany). Commercial Mössbauer source of ^{57}Co in rhodium matrix (Ritverc isotope products, Saint Petersburg, Russia) with an activity of about 40 mCi was used as the γ-radiation source. Low-temperature measurements were carried out with a continuous flow cryostat (model CFICEV from ICE Oxford, UK), equipped with Cryo-Con temperature controller (Model 32B); the sample temperature was kept with an accuracy of ± 0.5 K. The absorber was prepared by uniformly packing the sample under study into a holder closed by thin aluminium foil. The experimental spectra were least-squares fitted with the assumption that line shapes are Lorentzian to yield the hyperfine parameters, namely isomer shift (IS), quadrupole splitting (QS), and hyperfine field (HF). A metallic-iron foil at RT was used for velocity calibration of the Mössbauer spectrometer. Isomer shifts were referred to α-Fe at RT. The magnetization was measured on the PPMS-9 device in the temperature range from 10 to 400 K in zero-field-cooled (ZFC) and field-cooled (FC) regimes. The magnetic hysteresis loops were measured in the field range 1T.

Results and discussion

In the first experiment, the Fe^{3+}/Ni^{2+} ratio on the impregnation step was taken as 2/1, i.e. theoretical for invar. After annealing the as-prepared Fe^{3+}/Ni^{2+}-GO composite, no binary Fe/Ni-NPs were formed, but only particles of individual metals (see section 1 of ESI, Fig. S1, S2, S3, S4, Table S1). The Fe/Ni ratio in the product was >9/1. This is because the Fe^{3+} and Ni^{2+} ions are sorbed by GO unequally,

Published on 11 June 2019. Downloaded by Kazan State University on 6/18/2019 8:28:08 AM.

CrystEngComm Accepted Manuscript

This journal is © The Royal Society of Chemistry 20xx

View Article Online
DOI: 10.1039/C9CE00580C

Published on 11 June 2019. Downloaded by Kazan State University on 6/18/2019 8:28:08 AM.

CrystEngComm Accepted Manuscript

due to the difference in the ionic charge, and in the ability of the ions to serve as Lewis acids to form coordinate-covalent bonds with the oxygen functional groups of GO.[21] This is why, as the next step we assessed the affinity of the two ions toward GO. See SI section 2, and Fig. S5, S6 for details. Based on the obtained data, in the new experiment, the ratio of the two ions Fe^{3+}/Ni^{2+} during the impregnation step was taken as 1/7.

The TGA analysis of the newly prepared Fe^{3+}/Ni^{2+}-GO (Fig. 1) in synthetic air (O_2/N_2) shows that Fe^{3+}/Ni^{2+}-GO leaves 18% residue, attributable, according to XRD, to iron (III) and iron (II, III) oxides, and to nickel (II) oxide (Fig. S7a). After the functionalization of GO with metal ions, the thermal decomposition temperature of the GO's functional groups decreases from 170–230 ºC for pure GO to 146–190 ºC for Fe^{3+}/Ni^{2+}-GO. This is not typical behaviour, and our previous observations indicate that binding of Fe^{3+} and Pd^{2+} stabilizes GO functional groups against decomposition.[19, 20] The burning temperature of the carbon frame also shifts toward lower values: from 450–550 ºC to 320–450 ºC, suggesting that metal nanoparticles, forming on GO surface during the annealing, accelerate burning of tpGO.

The XRD pattern of Fe^{3+}/Ni^{2+}-GO (Fig. S7b) shows a strong peak centred at 2θ = 10.2°, corresponding to (001) reflection of GO. Importantly, the XRD pattern does not contain any reflexes associated with $Fe(NO_3)_3$ and $Ni(NO_3)_2$. According to the XPS data, no nitrogen was detected (see Fig. S8). The N1s XPS signal for nitrate, if present, should manifest at ~405 eV. Thus, the XRD and XPS data show that all the nitrate anions were removed from the composite during the impregnation step.

The C1s XPS spectrum of Fe^{3+}/Ni^{2+}-GO (Fig. 2a) is in general typical for graphene oxide. The spectrum is dominated by the component centred at 284.8 eV that is attributed to the C-C bonded atoms. The peak at 287.1 eV is associated with the carbon atoms of epoxides and tertiary alcohols, and it has lower intensity, compared to the 284.8 eV peak. This fact indicates that GO is partially reduced during the impregnation step. After annealing, the C1s XPS spectrum for Fe/Ni-NP_tpGO is composed of one single component centred at 284.8 eV.

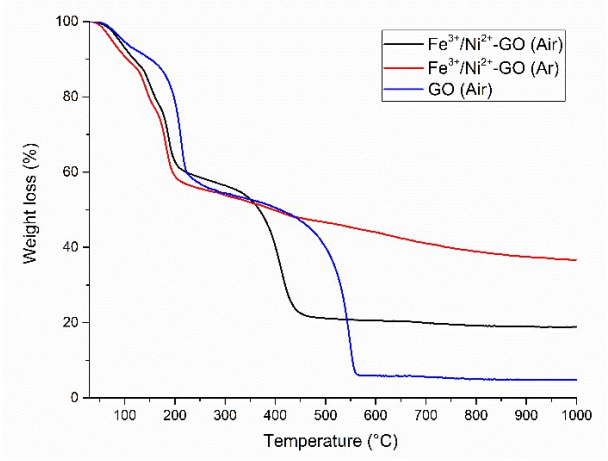

Fig. 1. Characteristics of Fe^{3+}/Ni^{2+}-GO: the TGA data in Ar and in synthetic air. Comparison to pure GO is given for reference purposes.

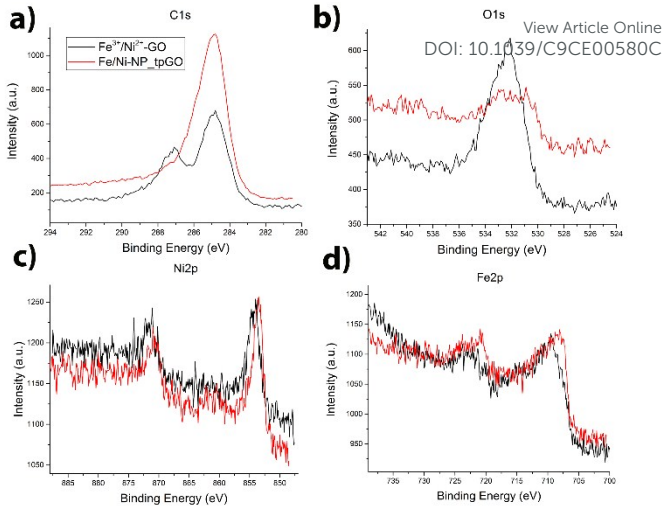

Fig. 2. The XPS spectra for Fe^{3+}/Ni^{2+}-GO (black curves) and Fe/Ni-NP_tpG0 (red curves). (a) C1s; (b) O1s; (c) Ni2p; (d) Fe2p.

The peak at 287.1 eV turns into shoulder, signifying that the oxygen functionalities have been decomposed. This correlates well with the O1s spectrum (Fig. 2b), which intensity decreases with annealing. The Ni2p XPS spectrum for Fe^{3+}/Ni^{2+}-GO (Fig. 2c) with the peaks at 854.1 eV and 871.0 eV indicates that nickel is in the oxidized form. The shift of the peaks toward lower binding energy for Fe/Ni-NP_tpGO can be interpreted as reduction of nickel (II) ions to nickel metal. The same dependence is observed for the Fe2p XPS spectrum of Fe/Ni-NP_tpGO (Fig. 2d), with the peak position at 708 eV. This value is typical for the Fe2p signal in the Fe/Ni invar alloys.[22] Based on the XPS data, the Fe/Ni-NP_tpGO sample contains iron and nickel in the ratio 65%:35%, which is close to the invar composition. This XPS data correlates with the XRD and Mössbauer spectroscopy data.

The XRD pattern of Fe/Ni-NP_tpGO is shown in Fig.3. The diffraction peaks at 2θ values of 43.4°, 50.6°, and 74.5° can be indexed to the (111), (200), and (220) crystal planes of the face-centered cubic (fcc) Fe/Ni alloy, which are very similar to those of fcc Fe.

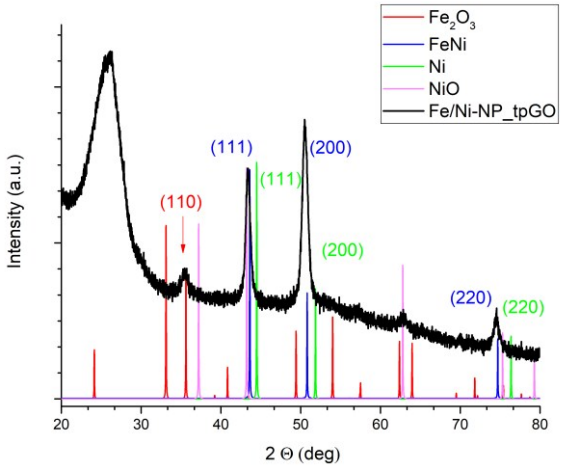

View Article Online
DOI: 10.1039/C9CE00580C

Fig. 3. Powder XRD pattern of Fe/Ni-NP_tpGO; the diffraction patterns for bulk forms of Fe/Ni, Fe_2O_3, Ni, and NiO are given as reference.

Concerning the low angle region, only the iron oxide reflex is detected at 35.5° 2θ in the XRD diffraction pattern. The broad peak at around 2θ value of 25.9° is a typical (002) graphitic reflex for "thermally reduced" GO. The weak signals at ~36° and ~63° 2θ can be attributed to Fe_2O_3 and NiO, respectively. The metallic nickel phase is not detected. This indicates that almost all the nickel atoms have been incorporated into the Fe/Ni alloy lattice with formation of solid solution, and do not form separate crystallites.

The Mössbauer spectroscopy data provide more information about the environment of iron atoms in the as-formed solid solution. The absorption spectra acquired at 300 K and at 80 K are shown in Fig. 4. The hyperfine parameters obtained by fitting the Mössbauer spectra are presented in Table 1. The Mössbauer spectrum, acquired at 300 K (Fig. 4a), was fitted by two sextets with different hyperfine magnetic field distributions and one singlet. The central narrow singlet with IS = -0.05 mm/s can be attributed to γ-Fe in which each iron atom is surrounded by 12 neighbouring iron atoms, as in the bulk fcc lattice of γ-Fe.[20] The hyperfine magnetic field distribution (HMFD) with lower average hyperfine field (Sextet 2), $\overline{H}$ = 214 kOe, is most likely related to the fcc phase of the alloyed binary Fe/Ni-NPs. The shape of the HMFD function shows that it can be decomposed into several components (Fig. 4b), which appear due to the different local surroundings of the Fe atoms in the fcc lattice. The best fit of this curve was achieved under the assumption of the binomial distribution of the atoms surrounding the Fe atom in the alloy.[23]

Table 1 The fitting parameters of the Mössbauer spectra: average hyperfine magnetic field $\overline{H}$, isomer shift $\overline{\delta}$, and contribution of components in spectrum for investigated compounds (%).

Component	Assigned to phase	$\overline{\delta}$ (mm/s), ±0.01 mm/sec	$\overline{H}$ (kOe), ±1 kOe	Contribution (%), ±0.5%
300 K				
Singlet	γ-Fe	-0.05		13
Sextet 1	Iron oxides	0.20	483	18
Sextet 2	Fe/Ni	0.01	214	69
300K, 2 kOe				
Singlet	γ-Fe	0.02		12
Sextet 1	Iron oxides	0.29	475	19
Sextet 2	Fe/Ni	0.01	212	69
80 K				
Singlet	γ-Fe	0.1		7
Sextet 1	Iron Oxides	0.35	509	19
Sextet 2	Fe/Ni	0.06	287	74

The insert in Fig. 4b shows the distribution of probability *P(n)* that Fe atom has *n* Fe atoms as the nearest neighbours in Fe/Ni-NPs. The maximum probability is observed when *n* is equal to 8, which corresponds to the phase with the Fe/Ni ratio equal to 67%:33%.[24, 25] A sextet with pronounced external lines at high velocities (Sextet 1) was also processed using the distribution of hyperfine magnetic fields. This sextet is related to the iron (III) oxide. The average values of the fields are 483 kOe and 475 kOe, when measured without and with the applied external magnetic field, respectively. Application of

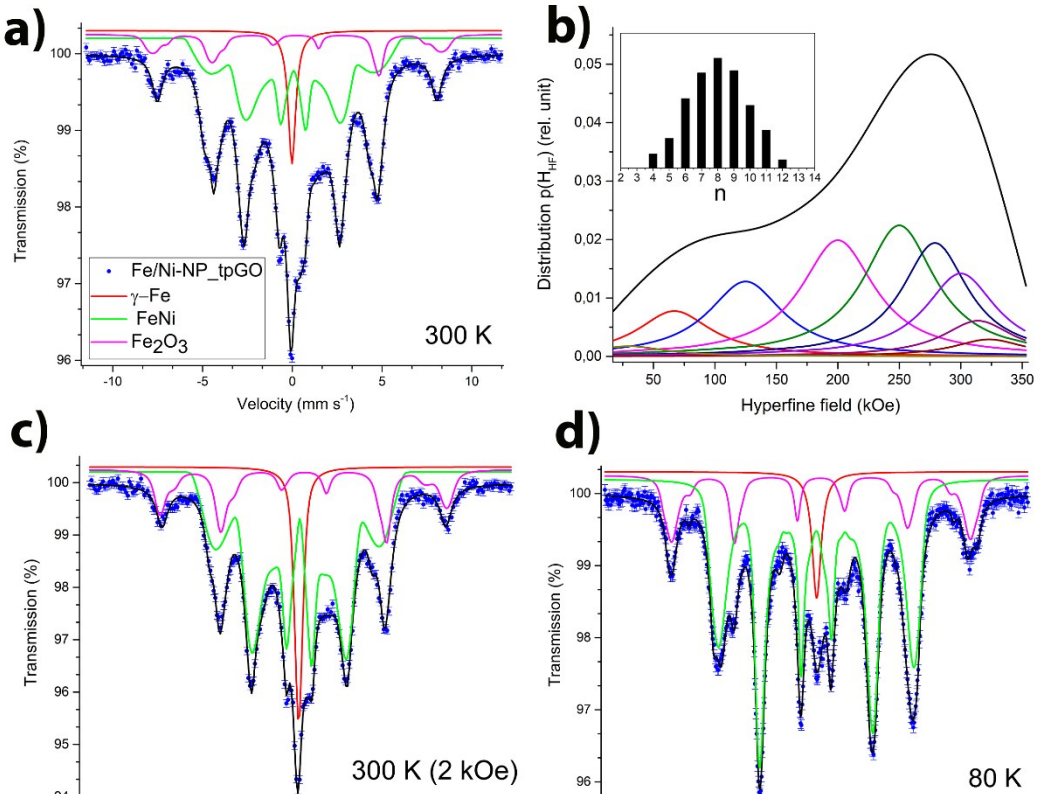

Fig. 4. Mössbauer characterization of Fe/Ni-NP_tpGO: a) Mössbauer spectrum at 300 K, and b) the corresponding hyperfine magnetic field distribution for sextet 2 and probabilities P(n) (insert); c) Mössbauer spectrum at 300 K in the applied magnetic field; d) Mössbauer spectrum at 80 K.

Published on 11 June 2019. Downloaded by Kazan State University on 6/18/2019 8:28:08 AM.

CrystEngComm Accepted Manuscript

This journal is © The Royal Society of Chemistry 20xx

Please do not adjust margins

View Article Online
DOI: 10.1039/C9CE00580C

Published on 11 June 2019. Downloaded by Kazan State University on 6/18/2019 8:28:08 AM.

the external magnetic field does not lead to noticeable changes in the shape of the Mössbauer spectrum (Fig. 4c) and in the content of the components. We can only note a small increase in the content of iron oxide, and some reduction in the content of fcc-Fe (Table 1).

More significant changes in the shape of the spectrum are observed when measured at 80 K (Fig. 4d). The relative area of the singlet decreases from 13% at room temperature to 7% at liquid nitrogen temperature (Table 1). The decrease in the singlet area can be explained by the fact that at room temperature, in this velocity region, in addition to the absorption line corresponding to γ-Fe particles, there were absorption lines of superparamagnetic iron oxide (~ 1%) and the Fe/Ni alloy particles (~ 5%), for which the transition temperature to a magnetically ordered state is below room temperature.

To summarize, the Mössbauer spectroscopy data show that the annealing-reduction method leads to the formation of the binary Fe/Ni-NPs. Their composition is close to that in invar. The Mössbauer spectrum of these nanoparticles is a set of magnetic sextets whose intensities is a function of the binomial distribution.

Fig. 5 shows the SEM image of Fe/Ni-NP_tpGO, and the associated particle size distribution histogram. This histogram indicates two maximums in the range of 20 nm to 30 nm, and 90 nm to 110 nm. This suggests that the sample contains two types of NPs. NPs with the size of 20-30 nm have circular shape that looks like iron (III) oxide nanoparticles. [26, 27] The larger nanoparticles have simple forms of cubic singony that can be attributed to the fcc Fe/Ni crystal.

Fig. 6a shows the ZFC–FC (H = 0.01 T) temperature dependence of the magnetization for Fe/Ni-NP_tpGO in the range 5–400 K. The high temperature value for the magnetization, measured after zero-field cooling, is very close to the value for the magnetization, measured after field cooling. However, these curves do not intersect at temperature region of 300 K, suggesting the ferromagnetic behaviour of the composite at room temperature. The blocking temperature is higher than 400 K, since there is no peak in the ZFC magnetization curves. Such behavior suggests that the superparamagnetic phase contribution is very low.

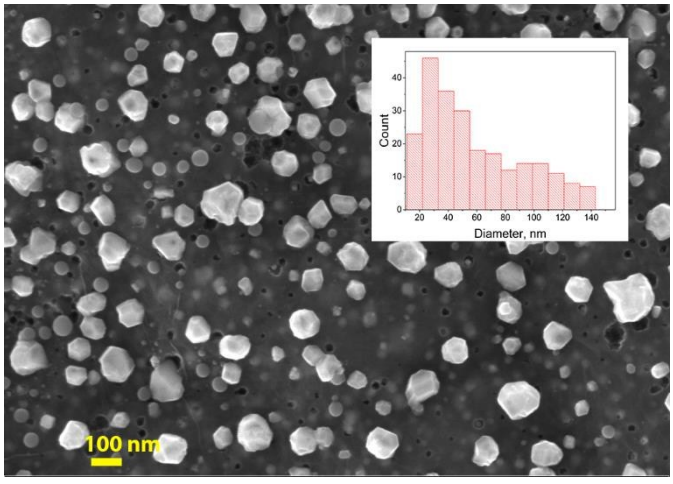

Fig. 5. SEM image (50 K magnification) of Fe/Ni-NP-tpGO and associated particle size histogram (insert)

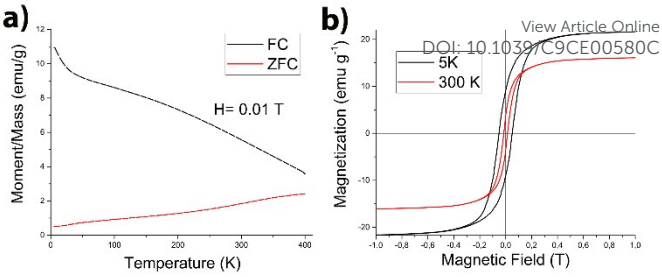

Fig. 6. Magnetic properties of Fe/Ni-NP_tpGO. a) Magnetic hysteresis loops at 5 K and 300 K. b) ZFC-FC curves.

Magnetic hysteresis loops of Fe/Ni-NP_tpGO were investigated at 5 K and 300 K with the applied field -1T < H < 1T (Fig 6 b). The ferromagnetic behavior is due to the high content of Fe/Ni-NPs. The saturation magnetization and coercivity values are presented in Table 2. The magnetization is calculated per the unit mass of the sample since we do not know the exact amount of the magnetic phase in it. This is why, we did not estimate each magnetic moment per an atom (μ) with respect to the value of the Bohr magneton. The general shape of the M(H) loop and the non-zero coercivity suggest that Fe/Ni_NP-tpGO is a soft magnetic material, and the majority of the nanoparticles are in a magnetically ordered state that is also supported by the Mössbauer spectroscopy.

Table 1 Magnetic data of the Fe/Ni_Np-tpGO composite at 5 K and 300 K

Temperature, °C	H_c, T	M_s, emu/g
5 K	0.051	21
300 K	0.014	16

Conclusions

The binary alloyed Fe/Ni nanoparticles have been synthesized on the graphene oxide support by the two-step synthetic method. The impregnation step results in formation of the Fe^{3+}/Ni^{+2}-GO composite, where the two metals exist mostly in the form of Fe^{3+} and Ni^{2+} ions chemically bound to GO via the coordinate covalent bonding. After annealing, the metals are reduced, and form the alloyed nanocrystals. Fe/Ni-NPs with the metals ratio close to that in the invar alloy (~65% of iron, ~35% of nickel) have been formed, which was confirmed by XPS, XRD, and Mössbauer spectroscopy. Other phases are the iron oxide impurities and γ-Fe in the quantity of 19% and 7%, respectively. According to XRD, there are no traces of individual nickel or nickel oxide in the sample, suggesting that nickel is alloyed with iron, and the Fe/Ni-NPs are formed. Magnetic measurements show that majority of the Fe/Ni-NPs are in a magnetically ordered state, and the composite is a soft magnet in nature, which provides an opportunity for magnetic storage.

Conflicts of interest

There are no conflicts to declare.

CrystEngComm Accepted Manuscript

View Article Online
DOI: 10.1039/C9CE00580C

Acknowledgements

This research was conducted with support of the Russian Science Foundation, Grant #16-13-10291. The SEM images were acquired using the equipment of the Interdisciplinary Centre for Analytical Microscopy, Kazan Federal University.

Notes and references

1. H. H. Al-Kayiem, S. C. Lin and A. Lukmon, *Nanoscience and Nanotechnology - Asia*, 2013, **3**, 60-71.
2. J. Spivey, *Metal nanoparticles for catalysis: advances and applications*, Royal society of chemistry, 2014.
3. H. Jahangirian, E. G. Lemraski, T. J. Webster, R. Rafiee-Moghaddam and Y. Abdollahi, *International Journal of Nanomedicine*, 2017, **12**, 2957-2978.
4. A. Sharma, A. K. Goyal and G. Rath, *Journal of Drug Targeting*, 2018, **26**, 617-632.
5. M. Benelmekki, *Designing hybrid nanoparticles*, 2015.
6. F. Yin, Z. W. Wang and R. E. Palmer, *Journal of the American Chemical Society*, 2011, **133**, 10325-10327.
7. Y. H. Xu and J. P. Wang, *Advanced Materials*, 2008, **20**, 994-999.
8. L. O. P. Borbón, *Computational studies of transition metal nanoalloys*, Springer Science & Business Media, 2011.
9. C. Langlois, D. Alloyeau, Y. Le Bouar, A. Loiseau, T. Oikawa, C. Mottet and C. Ricolleau, *Faraday Discussions*, 2008, **138**, 375-391.
10. I. A. Abrikosov, O. Eriksson, P. Söderlind, H. L. Skriver and B. Johansson, *Physical Review B*, 1995, **51**, 1058-1063.
11. J. L. Corbacho, J. C. Suárez and F. Molleda, *Welding International*, 1998, **12**, 966-971.
12. M. Yakout, A. Cadamuro, M. Elbestawi and S. C. Veldhuis, *The International Journal of Advanced Manufacturing Technology*, 2017, **92**, 2081-2098.
13. N. J. Harrison, I. Todd and K. Mumtaz, *Journal of Materials Science*, 2017, **52**, 10517-10525.
14. C. Qiu, N. J. Adkins and M. M. Attallah, *Acta Materialia*, 2016, **103**, 382-395.
15. J. T. Strauss and M. J. Stucky, 2016.
16. X. Liu, Z. Ou, D. Geng, Z. Han, J. Jiang, W. Liu and Z. Zhang, *Carbon*, 2010, **48**, 891-897.
17. X.-W. Wei, G.-X. Zhu, J.-H. Zhou and H.-Q. Sun, *Materials chemistry and physics*, 2006, **100**, 481-485.
18. S. Bai, X. Shen, G. Zhu, Z. Xu and J. Yang, *CrystEngComm*, 2012, **14**, 1432-1438.
19. A. A. Khannanov, A. R. Valimukhametova, A. G. Kiiamov, I. R. Vakhitov and A. M. Dimiev, *ChemistrySelect*, 2017, **2**, 10546-10554.
20. A. Khannanov, A. Kiiamov, A. Valimukhametova, D. A. Tayurskii, F. Börrnert, U. Kaiser, S. Eigler, F. G. Vagizov and A. M. Dimiev, *Journal of the American Chemical Society*, 2018, **140**, 9051-9055.
21. R. R. Amirov, J. Shayimova, Z. Nasirova and A. M. Dimiev, *Carbon*, 2017, **116**, 356-365.
22. A. Chourasia and D. Chopra, *Nuclear Instruments and Methods in Physics Research Section B: Beam Interactions with Materials and Atoms*, 1989, **40**, 376-378.
23. J. Müller and J. Hesse, *Zeitschrift für Physik B Condensed Matter*, 1983, **54**, 35-42.
24. M. Kądziołka-Gaweł, W. Zarek, E. Talik and E. Popiel, *Acta Physica Polonica A*, 2008, **6**, 1493-1500.
25. C. Johnson, M. Ridout and T. Cranshaw, *Proceedings of the Physical Society*, 1963, **81**, 1079.
26. Q. Meng, Z. Wang, X. Chai, Z. Weng, R. Ding and L. Dong, *Applied Surface Science*, 2016, **368**, 303-308.
27. J. Lian, X. Duan, J. Ma, P. Peng, T. Kim and W. Zheng, *ACS nano*, 2009, **3**, 3749-3761.

Published on 11 June 2019. Downloaded by Kazan State University on 6/18/2019 8:28:08 AM.

CrystEngComm Accepted Manuscript

This journal is © The Royal Society of Chemistry 20xx

View Article Online
DOI: 10.1039/C9CE00580C

Published on 11 June 2019. Downloaded by Kazan State University on 6/18/2019 8:28:08 AM.

Graphical Abstract

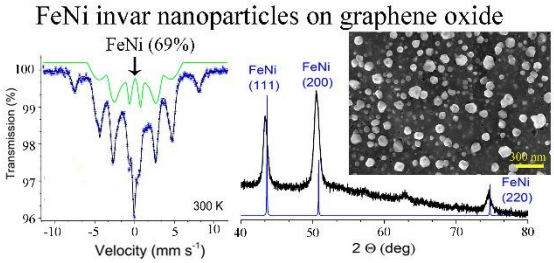

The alloyed binary invar-like FeNi nanocrystals are synthesized on the surface of graphene oxide in the two-step impregnation-annealing procedure.

CrystEngComm Accepted Manuscript